Volume **1** (2): 2023 **page 52-61**, https://doi.org/10.59785/tjhest.v1i2.25 https://tamjed.com/

Convolutional Neural Networks for breast cancer detection using regions of interest from infrared images

Prof. Dr. Sudan Jha
Department of Computer Science and Engineering, School of Engineering,
Kathmandu University, Nepal. E-mail: sudan.jha@ku.edu.np

Mamoon Fattah Khalf
Department of physics, University of Samarra,Iraq
E-mail: Mamoun42@uosamarra.edu.iq

Karthick.M
Department of Computer science and engineering, Nandha college of Technology,
Tamilnadu, India, E-mail: magukarthik@nandhatech.org

Received: 11/06/2023
Accepted for publication: 30/07/2023
Published: 04/08/2023

Abstract

Breast cancer is the most common cancer among women in Iraq and worldwide. The incidence in young women has been increasing over the years, and the gold standard test for diagnosis, mammography, is contraindicated for people under 40. Thermography appears in this scenario as a promising technique for early detection and a higher survival rate in this group of women. The analysis of thermographic images by Convolutional Neural Networks has good results in increasing the reliability and sensitivity of diagnoses. This work uses the Densenet201 and Resnet50 networks based on 72 images of different patients, 38 of whom are sick and 38 healthy. These images underwent pre-processing before being analyzed, and in one of the pre-processing steps, there was a manual clipping of only the region of interest of the breasts, intending to evaluate whether detection is superior to the image whole. The best average accuracy rate was obtained with the Densenet201 network, learning rate of 0.001 and 30 epochs, which reached 89%. Regarding the F1-score, the network with the best performance was Resnet50, with a learning rate of 0.0001 and 30 epochs, which reached 76%.

Keywords: Breast cancer, Artificial Intelligence, Neural Networks, Densenet, Resnet, Infrared Thermography.

1. Introduction

Breast cancer is the most frequent cancer among women worldwide, not only in Iraq. Although the frequency is higher in women over 50, incidences in younger women have increased in recent years. Early detection is critical since the

chances of treating breast cancer decrease drastically if the disease is not found in its early stages. Currently, several imaging tests are used for screening or aiding in the complementary diagnosis of this type of neoplasm, with mammography being the most common of them. Mammography is a test recommended by the WHO for women over 40 years old only because the ionizing radiation used in the test is considered a risk factor for breast cancer in younger women. Despite having a sensitivity of around 85%, this test is influenced by variables such as the woman's age and the density of her breasts. This is because the younger women are, the denser their breasts are, and the differential visual analysis of mammography of a dense breast is more susceptible to mistakes [1].

A non-invasive, non-contact, low-cost, quick, painless, and compassionate technique has recently gained attention. This technique is appropriate for women of all ages, with any breast size or density, and for young and pregnant women. This is thermography, based on the principle that metabolic activity and vascular circulation are almost always more significant in cancerous tissues and the area around a breast tumor development than in normal breast tissue [2].

In thermography, by means of infrared radiation, a specialized camera can detect the heat that arrives from the inside of the tissue to the skin's surface through thermal conduction. This heat is illustrated as a graph with a color gradient so that the region where the cancer is located has a color that represents the highest temperature [3]. This procedure is called infrared thermography (IRT).

IRT for breast cancer detection has its first use reports in the 50s. However, the results obtained then needed to be more satisfactory due to technological limitations. However, since the 2000s, with the improvement of infrared cameras and the advancement of artificial intelligence (AI), infrared thermography has shown to be a promising technique for detecting breast cancer [4].

In this sense, this work will study using AI techniques combined with infrared images to detect breast cancer. The evaluated Neural Networks were Densenet201 and Resnet50 [5]. The best average accuracy rate was obtained with the Densenet201 network, learning rate of 0.001 and 30 epochs, which reached 89%. Regarding the f1-score, the network with the best performance was Resnet50, with a learning rate of 0.0001 and 30 epochs, which reached 76%.

Despite being attractive, breast cancer diagnoses using only thermographic images are still not entirely accepted by the medical community, being used as complementary exams. However, given the increasing number of breast cancer cases in younger women and the limitations of mammography in this type of public, it is essential to reframe this medical concept.

Several image analysis techniques can be used in order to increase the reliability and sensitivity of these diagnoses, and the ones with the best results are those based on Convolutional Neural Networks (CNN). Therefore, this work proposes an intelligent breast cancer detection system based on the analysis of thermographic images and CNN algorithms, in which the results will indicate the potential of this approach to replace conventional exams, such as mammography. There are already some works in the same line of research for the detection of breast cancer through thermographic images:

An algorithm for extracting characteristic features of the breast based on biodata, picture analysis, and image statistics was proposed [6]. These traces were recovered from thermal images acquired by a thermal camera and used in convolutional neural networks (CNNs) optimized by the Bayes algorithm to classify breast images as usual or suspicious. For a set of 140 thermal pictures, this proposed algorithm achieved an accuracy rate of 98.95%.

Zuluaga-Gomez et al. (2020) [7] conducted an intriguing investigation to demonstrate that computer-aided diagnostic (CAD) systems based on CNNs are faster, more reliable, and more resilient than other methodologies. In order to do so, they researched the impact of data pre-processing, data expansion, and database size vs a proposed set of CNNs models.The CNN models in this work outperformed many state-of-the-art architectures, including ResNet50, SeResNet50, and Inception, regarding accuracy (92%) and F1-score (92%). They also proved that a CNN model that uses data augmentation techniques obtains the same performance metrics as a CNN that uses a database up to 50% larger [7].

Another intriguing investigation was conducted by a group of researchers [8]. They trained CNN models (ResNet101, DenseNet, MobileNetV2, and ShuffleNetV2) using the DMR-IR database image dataset [11]. The learning rate was set to 0.001 during training, and three distinct epochs were employed for training iterations: 10, 20, and 30. The training results showed that ResNet101 and DenseNet with deep networks achieve 100% accuracy in 10 epochs, whereas MobileNetV2 and ShuffleNetV2 require 20 and 30 epochs of training, respectively. DenseNet was able to accurately categorize the complete test dataset during the performance evaluation of each pre-trained model [8].

To understand this work, knowledge of some concepts and definitions is necessary. They will be presented in this section.

2. Infrared Images

Infrared radiation was discovered by studies carried out by astronomer Willian Herschel. After repeating the experiment carried out by Isaac Newton when he scattered sunlight with the help of a prism, Herschel looked for the color with the highest temperature by focusing the beams on a thermometer. That is when he realized that the region with a

frequency slightly lower than that of red light was the hottest region [9]. The name infrared comes precisely from the fact that the frequency of radiation is lower than the frequency of red light, which, in turn, is the lowest frequency captured by the human eye [9].

The principle used by thermography is that everybody with a temperature above absolute zero emits infrared radiation [10]. In medicine, when cells present anomalies, alterations in the metabolism and immune response cause elevations in the temperature of the affected regions. With that, a specialized camera (Figure 1a) captures these temperature differences through excitations of the electromagnetic spectrum (Figure 1b).

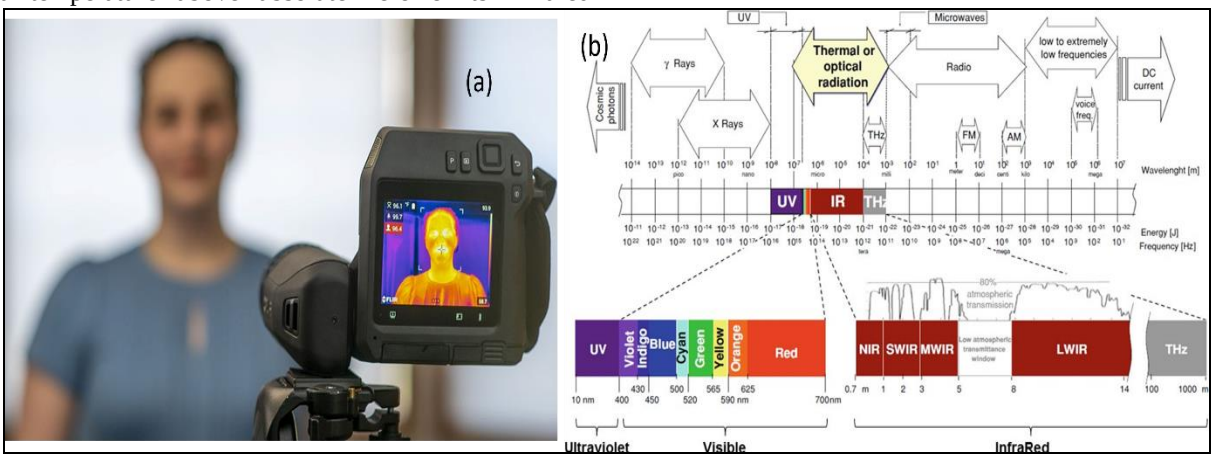

Figure 1: (a) – Example of the thermographic camera ; (b) Functioning of an electromagnetic spectrum

3. Convolutional Neural Networks (CNN)

A variant of the multilayer perceptron, the convolutional neural network (CNN) is an architecture based on a biological data processing process. This type of network is mainly used in detection, classification, and recognition applications in images and videos. CNNs are divided into stages, in which, generally, the first ones are constituted by convolution and pooling layers, followed by wholly connected or softmax layers. NNs, based on feedforward neural networks, have great potential for analyzing and classifying images. Two characteristics are necessary to be highlighted about the CNN classifiers: convolution and pooling.

Convolution makes it possible to attribute different functions and weights discovered by the algorithm during the neural network training process, to generate the feature map in each hidden layer. The pooling layer is used to reduce and simplify data, making the generalization of information more effective. Early stopping is a technique used to prevent over-fitting a network by limiting the number of epochs. In deep networks, epochs refer to the number of times a learning algorithm sees the complete data set. Finally, transfer learning (or transfer learning) has the idea of using knowledge learned in a more extensive database applied to other databases; the learning process does not start from scratch. Bearing this in mind, in this work, the CNNs were developed to accept as input images from the region of interest from the DMR-IR database [11] and return the class of input images: cancer or healthy (non-cancer). Next, we present the two networks used in this work and the metrics used for comparisons.

The mutations described in the previous section can occur in breast cells, resulting in breast cancer. This type of carcinoma is subdivided into fibroadenoma (benign neoplasm), ductal carcinoma, and lobular carcinoma (malignant neoplasm). For the detection of breast cancer, several clinical exams are performed, the most frequently found in clinical practice being self-examination, followed by complementary exams such as mammography and ultrasound [9].

3.1 Resnet 50

After a number of layers, the accuracy of a neural network tends to deteriorate, and Resnet's significant differential with other networks is used to prevent this degradation. Residual learning uses input values to influence the final output of each block, as shown in Figure 2a.[12]

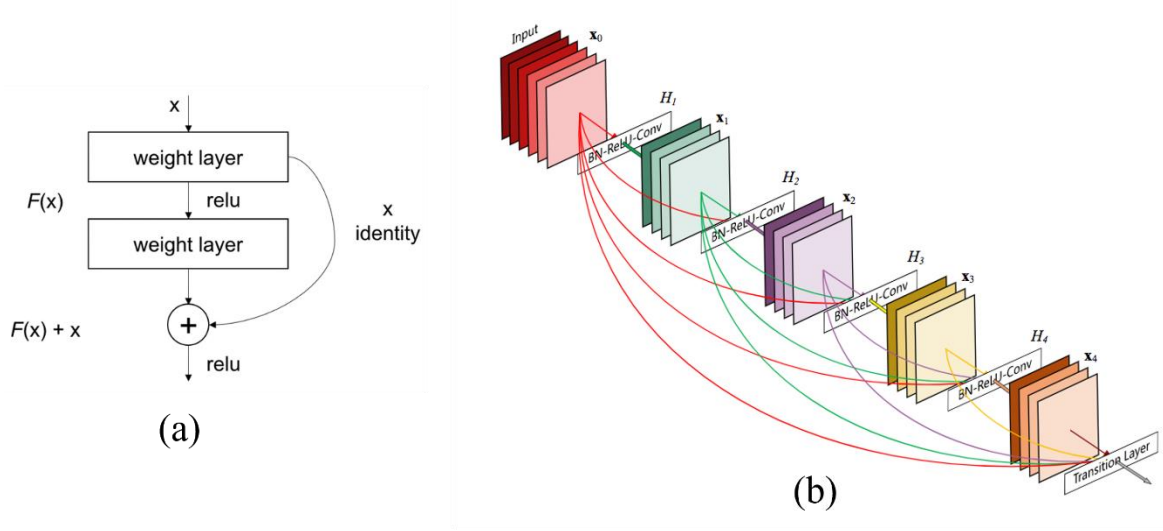

Figure 2: (a) – The operating model of a Resnet50; (b) - The operating model of a DenseNet201

3.2 Densenet 201

Another way to prevent neural network degradation after a large amount of layers is proposed by Densenet, in which each layer receives all previous feature maps as input, making it a remarkably optimized network but a cumbersome and difficult network to debug be processed. Figure 2b presents an example from Densenet [13].

3.3 Evaluation metrics

To evaluate the classifiers, several metrics can be used, the most common and those used in this study being sensitivity, specificity, accuracy, and the F1-Score. However, in order to understand them, it is necessary to understand concepts in the area of result health:

- True positive (TP): number of samples labeled as diseased that are identified as diseased.
- True negative (TN): number of samples labeled as healthy that are identified as healthy.
- False positive (FP): number of samples labeled as healthy that are identified as diseased.
- False negative (FN): number of samples labeled as diseased that are identified as healthy [14].

Based on these concepts, the metrics mentioned above are calculated, namely:

• Sensitivity: the ability to determine images labeled as diseased correctly.

$$\text{Sensitivity} = \frac{TP}{TP + FN}$$

• Specificity: the ability to determine images labeled as healthy correctly.

$$\text{Specificity} = \frac{TN}{TN + FP}$$

• Accuracy: the ability of the model to correctly differentiate the image in the healthy and sick classes, being the proportion of true positives and true negatives overall evaluated cases.

$$\text{Accuracy} = \frac{TP + TN}{TP + TN + FP + FN}$$

• Accuracy: determining true positives from all images labeled positive.

$$\text{Precision} = \frac{TP}{TP + FP}$$

F1-score: a harmonic mean between accuracy and sensitivity.

$$\text{F1} - \text{score} = \frac{2 * \text{Precision} * \text{Sensitivity}}{\text{Precision} * \text{Sensitivity}}$$

These metrics can be represented visually by the confusion matrix, or error matrix, each row represents the predicted class instances, and the columns represent the class itself (or vice versa) for a matrix of size NxN. We have the

example of the confusion matrix [15] of the 18 classifications as being pathological; in 77.8% of the times, the prediction was correct (14 times), and in 22.2%, they were wrong (4). For the 22 samples classified as being normal, in 72.7%, he hits (16), and in 27.3%, he misses (6). There is also accuracy information in the last line and in the last column: 75%. Sensitivity and specificity can be seen in the last line of the confusion matrix, with values of 70% and 80%, respectively. We can also extract the values of VP, FP, FN, and VN from the matrix; they are 14, 4, 6, and 16, respectively[15].

This work is developed to compare the performance of different CNNs in terms of the F1-Score and accuracy metrics in whole images and images only of the region of interest for detecting breast cancer and assess whether detection is superior in images only of the region of interest.

4 Methodology

This section describes the database used, details of pre-processing and processing to analyze the F1-Score, and accuracy rates of the chosen CNNs. Figure 4 presents the study methodology flowchart.

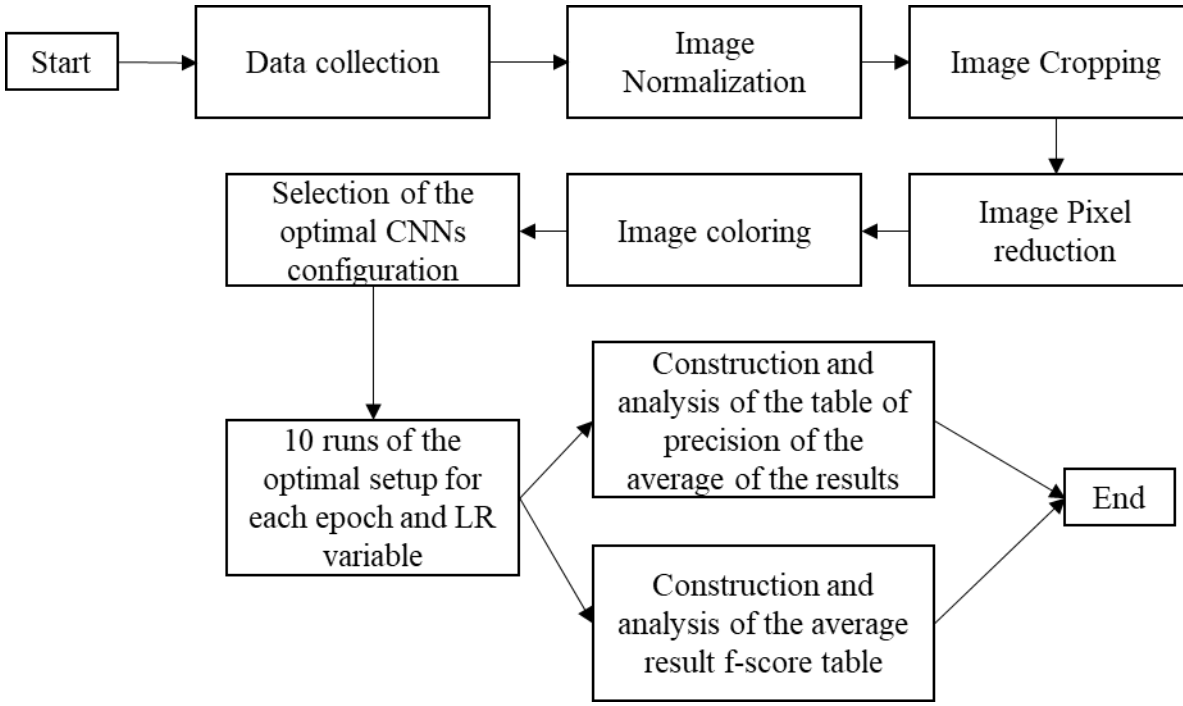

Figure 4: Study flowchart

4.1 Database

During this graduation project, the DMR-IR database initially proposed by Silva *et al*.,(2014)[11] and freely available at https://www.kaggle.com/datasets/asdeepak/thermal-images-for-breast-cancer-diagnosis-dmrir, which contains static and dynamic thermal images of at least 46 women with breast cancer and 192 without the condition, which were obtained using the FLIR camera SC-620 with a resolution of 640 x 480 pixels, where each pixel represents a temperature value. A still image is a single image of the patient (at a given time t). On the other hand, dynamic images are composed of a set of 22 images of the patient at different times but captured in sequence.

Each patient analyzed has 27 images, 22 of which are dynamically taken over 5 minutes, which were not used in this work, and five static images from different angles that have the region of interest, in poses: frontal (Images (a) of Figures 5a & b), left side of 45° (Images (b) of Figures 5a & b) and 90° (Images (d) of Figures 5a & b) and right side of 45° (Images (c) of Figures 5a & b) and 90° (Images (e) of Figures 5a & b). In the present study, only frontal static images were analyzed, and an essential detail about this database is that it does not indicate the position of the tumor; it only classifies the patient as "with cancer" or "without cancer." At the time of data collection, there were only 38 sick patients in the database; therefore, to balance it, only 38 healthy patients were analyzed, randomly chosen.

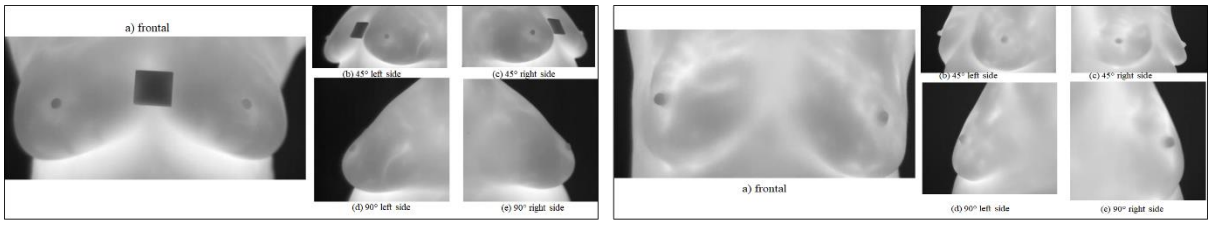

(a) (b)

Figure 5: (a)- Healthy person ; (b) Patient with breast cancer

4.2 Pre-processing

The pre-processing of the original thermal images took place in 4 steps. Such processing was necessary to pass the images as input to the CNNs.

Figure 6: Original thermal image.

4.2.1 1st Stage – Standardization: The images (Figure 7a)were normalized using the formula:

$$255 \times \frac{(P_{ij} - L)}{(H - L)} \quad (Eq. 4.1)$$

Where:

P_{ij} = pixel value of the image to be normalized in the row i and column j matrix.

H = highest value among all pixels of the image to be normalized

L = smallest value among all pixels of the image to be normalized.

2nd Stage – Trimming: The normalized images (Figure 7b) were manually cropped for region of interest (ROI) selection. The shape and size of the ROI were defined based on [16]

3rd Stage - Pixel Reduction: The images (Figure 7c) were reduced to 224 by 224 pixels because the networks were trained with images of this size.

4th Stage – Coloring: Finally, the networks used in this work were trained with color images. The network expects as input one matrix with three dimensions (a color image) (Figure 7d). Therefore, the normalized and reduced images of the region of interest were colored using the colormap jet as suggested by Cabioğlu (2020) [17]

4.3 Classification

At this stage of the work, the images that were processed in the previous steps are used for training and subsequent testing of the networks under analysis, so that 70% (n=26) of the database images are for training, 15% (n =6) for testing and 15% (n=6) for validation.

The Resnet 50 and Densenet 201 networks were already pre-trained, so transfer learning was applied. The authors (Gonçalves, Souza; Fernandes, 2021) [18] provided the implementations of the networks for application in this work. The networks have the following possible configurations:

a) 1 fully connected layer (resnet and densenet standard);

b) 2 layers completely connected with (256 input and output neurons of the first layer, 256 input and 2 output neurons of the second layer);

c) 2 layers completely connected with (512 input and output neurons of the first layer, 512 input and 2 output neurons of the second);

d) 2 layers completely connected with (1024 input and output neurons of the first layer, 1024 input and 2 output neurons of the second layer);

e) 3 completely connected layers of (4096 input and output neurons of the first layer, 1024 input and 2 output neurons of the second)

f) 3 layers completely connected with (4096 input and output neurons of the first layer, 4096 input and 2 output neurons of the second).

In the processing, after the initial execution of all the configurations, the configuration of the letter 'd' mentioned above was chosen due to its superior performance when compared to the others. After this choice, to analyze the results more faithful to reality, it was run 10 times for each CNN:

- 10 epochs and learning rates of 0.1, 0.01, 0.001, 0.0001
- 30 epochs and learning rates of 0.1, 0.01, 0.001, 0.0001

5 Results and Discussions

In this section, the results of the analyzes and the discussions regarding the average of the 10 executions of the configuration of the letter 'd', cited above, will be presented. A precision table and an F1-Score table were generated with these results.

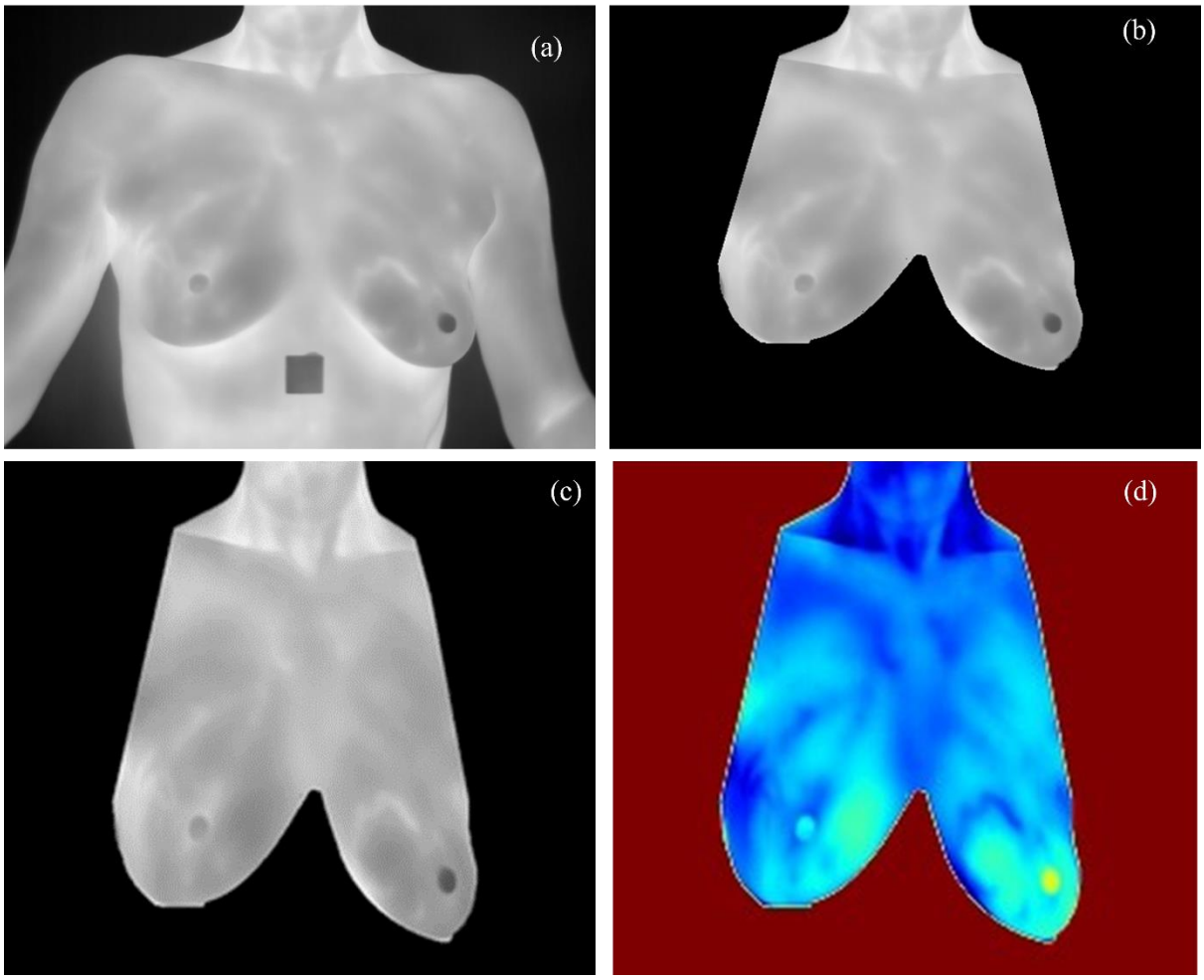

Figure 7: (a) Normalized thermal image; (b) Image of the normalized region of interest.; (c) Normalized and reduced image of the region of interest; and (d) Color image.

Table 1 : Accuracy table of the average of 10 executions of the CNNs with the 2 FC configuration with (1024.2)

	LR= 0.1		LR= 0.01		LR = 0.001		LR = 0.0001	
	epochs = 10	epochs = 30	epochs = 10	epochs = 30	epochs = 10	epochs = 30	epochs = 10	epochs = 30
resnet	0.3212	0.41	0.3012	0.7268	0.4821	0.8067	0.603	0.7935
densenet	0.38	0.3931	0.2545	0.8583	0.5433	0.8964	0.354	0.7167

Table 2 : Table of F1-Score of the average of 10 executions of the CNNs with the configuration 2 FC with (1024.2)

	LR= 0.1		LR= 0.01		LR = 0.001		LR = 0.0001	
	epochs = 10	epochs = 30	epochs = 10	epochs = 30	epochs = 10	epochs = 30	epochs = 10	epochs = 30
resnet	0.2769	0.4369	0.3009	0.7479	0.4471	0.6634	0.4338	0.7622
densenet	0.3894	0.3908	0.2956	0.6923	0.5138	0.725	0.4378	0.453

Through the precision table (Table 1), it was possible to notice that with the Resnet 50 and with the Densenet 201, good results were obtained with 30 epochs, except for when the learning rate was with a value of 0.1. This is because 0.1 is a very high learning rate, and when high, it changes the behavior of the network very quickly, making it difficult for it to obtain optimal results.

The best results were achieved with a learning rate of 0.001: in Resnet50, approximately 80.67% of accuracy was obtained, while in Densenet 201, approximately 89.64% of accuracy. However, the results of the present study were inferior to previous studies, with the same algorithms but with different study designs [7] they obtained a precision rate of 92% with the tested algorithms [6] the accuracy rate obtained was 98.95%; and in [8] obtained a 100% accuracy rate with the tested models.

The early stopping (early stop) in artificial intelligence, a famous technique to solve overfitting problems, instead of improving, worsened the results since the worst performances for the two CNNs were when the number of epochs of the algorithms was 10. It reached the worst results when the learning rate had a value of 0.01, with Resnet having the average precision of 10 executions at approximately 30.12% and Densenet at an average of approximately 25.45%. In the F1-Score table (Table 2), Resnet50 had a better performance with a learning rate 0.0001 and 30 epochs (76.21% approximately) than with the learning rate

0.001 and 30 epochs (66.33% approximately) when the best accuracy was achieved. Densenet201 continued to be superior, with 30 epochs and a learning rate of 0.001 (72.49% approximately). Both CNNs had better results than in [18], with the same configuration (2FC with (1024,2)), whose two algorithms obtained F1-score lower than 70%. However, also in [18], the final results were superior to the best of this study, both in Resnet (which had the best F1-Score result of approximately 83.33%) and in Densenet (in the best case obtained an F1-Score of approximately 92.30%).

In (Figure 8), one can check the evaluation metrics of the best result obtained with the Densenet 201 network with 30 epochs and a learning rate 0.001.

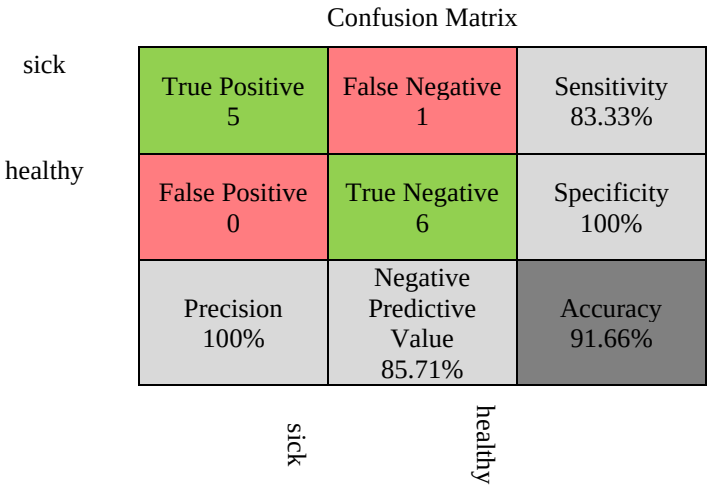

Figure 8: Confusion matrix of the best Densenet 201 result from the validation base

The f1-score of this best result was approximately 90.90%. With these values, it can be concluded that the limited sample size directly interferes with evaluating the algorithm's performance since, despite having 100% accuracy, 1 false negative result was enough to deteriorate the f1-score value. In (Figure 9), one can check the evaluation metrics of the best result obtained with the Resnet 50 network with 30 epochs and a learning rate of 0.001.

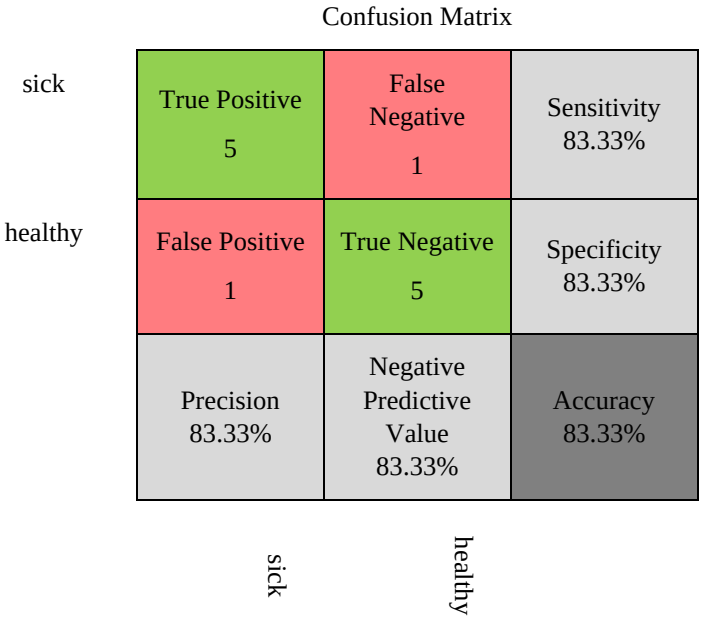

Figure 9: Confusion matrix of the best Resnet 50 result from the validation base

The f1-score of this best result was approximately 83.33%. With these values, it can also be concluded that the limited sample size directly interferes with evaluating the algorithm's performance since the metrics of precision and f1-score deteriorated with only 1 false negative value and 1 false positive value.

6 Conclusion

The use of thermographic images to detect breast cancer is a promising technique to aid in diagnosing this disease. In addition to providing early diagnosis, it is a painless, radiation-free technique, makes it possible to detect the disease in breasts where other techniques have limitations, and is inexpensive. Even though it is a promising technique, the application of CNNs on images with only the region of interest did not obtain better results (in the present study) than the whole images in relation to the evaluation metrics. However, further studies with more extensive databases are needed to confirm or even refute the present study's findings since images only of the region of interest would exclude many unnecessary details for artificial intelligence.

References

[1]. Mambou SJ, Maresova P, Krejcar O, Selamat A, Kuca K. (2018). Breast Cancer Detection Using Infrared Thermal Imaging and a Deep Learning Model. Sensors (Basel).18(9):2799. doi: 10.3390/s18092799.

[2]. Milosevic M, Jankovic D, Peulic A. (2014). Thermography based breast cancer detection using texture features and minimum variance quantization. EXCLI J. 13:1204-15

[3]. Abdel-Nasser, Mohamed, Antonio Moreno, and Domenec Puig. (2019). "Breast Cancer Detection in Thermal Infrared Images Using Representation Learning and Texture Analysis Methods" Electronics 8, no. 1: 100.

[4]. Satish G. Kandlikar, Isaac Perez-Raya, Pruthvik A. Raghupathi, Jose-Luis Gonzalez-Hernandez, Donnette Dabydeen, Lori Medeiros, Pradyumna Phatak, (2017). Infrared imaging technology for breast cancer detection – Current status, protocols and new directions, International Journal of Heat and Mass Transfer, Volume 108, Part B, Pages 2303-2320

[5]. Ravi V. (2022).Attention Cost-Sensitive Deep Learning-Based Approach for Skin Cancer Detection and Classification. Cancers (Basel). 14(23):5872. doi: 10.3390/cancers14235872.

[6]. Ekici S, Jawzal H. (2020). Breast cancer diagnosis using thermography and convolutional neural networks. Med Hypotheses.;137:109542. doi: 10.1016/j.mehy.2019.109542

[7]. Zuluaga-Gómez, Juan *et al*. (2019). A CNN-based methodology for breast cancer diagnosis using thermal images. Computer Methods in Biomechanics and Biomedical Engineering: Imaging & Visualization 9; 31 - 145.

[8]. Roslidar R. , SaddamiK. , ArniaF. , Syukri M. and Munadi,K. (2019). A Study of Fine-Tuning CNN Models Based on Thermal Imaging for Breast Cancer Classification, IEEE International Conference on Cybernetics and Computational Intelligence (CyberneticsCom), Banda Aceh, Indonesia, 2019, pp. 77-81,

[9]. Ring, E.F.J.. (2000). The discovery of infrared radiation in 1800. Imaging Science Journal The. 48. 1-8. 10.1080/13682199.2000.11784339.

[10]. E.Y.-K. Ng, (2009).A review of thermography as promising non-invasive detection modality for breast tumor,International Journal of Thermal Sciences,Volume 48, Issue 5, Pages 849-859,https://doi.org/10.1016/j.ijthermalsci.2008.06.015 .

[11]. da Silva Lincoln , Saade D, Sequeiros Olivera, Giomar, Silva Ari, Paiva Anselmo, Bravo Renato, Conci Aura. (2014). A New Database for Breast Research with Infrared Image. Journal of Medical Imaging and Health Informatics. 4:92-100. 10.1166/jmihi.2014.1226.

[12]. K. He, X. Zhang, S. Ren and J. Sun, (2016). Deep Residual Learning for Image Recognition, IEEE Conference on Computer Vision and Pattern Recognition (CVPR), Las Vegas, NV, USA, 2016, pp. 770-778, doi: 10.1109/CVPR.2016.90.

[13]. G. Huang, Z. Liu, L. Van Der Maaten and K. Weinberger (2017). Densely Connected Convolutional Networks," in 2017 IEEE Conference on Computer Vision and Pattern Recognition (CVPR), Honolulu, HI, USA, pp. 2261-2269. doi: 10.1109/CVPR.2017.243

[14]. Baratloo A, Hosseini M, Negida A, El Ashal G. (2015). Part 1: Simple Definition and Calculation of Accuracy, Sensitivity and Specificity. Emerg (Tehran). 3(2):48-9.

[15]. Chaves E, Gonçalves CB, Albertini MK, Lee S, Jeon G, Fernandes HC. (2020). Evaluation of transfer learning of pre-trained CNNs applied to breast cancer detection on infrared images. Appl Opt. 59(17):E23-E28. doi: 10.1364/AO.386037.

[16]. A Mohamed E, Gaber T, Karam O, Rashed EA. (2022). A Novel CNN pooling layer for breast cancer segmentation and classification from thermograms. PLoS One. 17(10):e0276523. doi: 10.1371/journal.pone.0276523.

[17]. Çağrı Cabıoğlu, Hasan Oğul. (2020). Computer-Aided Breast Cancer Diagnosis from Thermal Images Using Transfer Learning, Bioinformatics and Biomedical Engineering: 8th International Work-Conference, IWBBIO 2020, Granada, Spain, May 6–8, Proceedings Pages 716–726

[18]. C. B. Gonçalves, J. R. Souza and H. Fernandes, (2021). Classification of static infrared images using pre-trained CNN for breast cancer detection," 2021 IEEE 34th International Symposium on Computer-Based Medical Systems (CBMS), Aveiro, Portugal, pp. 101-106, doi: 10.1109/CBMS52027.2021.00094.